JOURNAL OF GEOPHYSICAL RESEARCH, VOL. 115, D00H11, doi:10.1029/2009JD012100, 2010



# HIRDLS and CALIPSO observations of tropical cirrus

Steven T. Massie,[1] John Gille,[1,2] Cheryl Craig,[1] Rashid Khosravi,[1] John Barnett,[3] William Read,[4] and David Winker[5]

Received 20 March 2009; revised 20 July 2009; accepted 24 September 2009; published 30 January 2010.

[1] High Resolution Dynamics Limb Sounder (HIRDLS) and Cloud-Aerosol Lidar and Infrared Pathfinder Satellite Observation (CALIPSO) measurements of cirrus frequency of occurrence in the upper tropical troposphere are quantified for September 2006 to August 2007. Monthly geospatial averages of cloud frequency of occurrence between 90 and 177 hPa are similar and correlate well with Microwave Limb Sounder (MLS) relative humidity with respect to ice (RHI) data, though clouds are present at individual RHI values less than 100%, due to the 5, 1, and sub-1 km vertical resolutions of the MLS, HIRDLS, and CALIPSO experiments. Seasonal variations in cloud frequency of occurrence are similar, with largest frequencies during winter (December–February). Though the CALIPSO and HIRDLS experiments employ nadir- and limb-viewing observational geometries, respectively, CALIPSO horizontal scales of cirrus are frequently larger than 100 km, and therefore similarities are present in the geospatial distributions of cloud occurrence. Isolated laminar cirrus is most prevalent away from the equator. The monthly patterns of HIRDLS and CALIPSO cloud occurrence are archived for useful comparisons to climate models.

**Citation:** Massie, S. T., J. Gille, C. Craig, R. Khosravi, J. Barnett, W. Read, and D. Winker (2010), HIRDLS and CALIPSO observations of tropical cirrus, *J. Geophys. Res.*, *115*, D00H11, doi:10.1029/2009JD012100.

## 1. Introduction

[2] Tropical cirrus in the upper troposphere is of interest because it plays an important role in the microphysical processes that determine how much water vapor is transported from the upper troposphere into the lower stratosphere, and in the radiative processes of the upper troposphere. *Jensen and Pfister* [2004] note that the details of how air enters the stratosphere, and the details of the dehydration processes, are not well understood. The efficiency of dehydration by cloud formation depends upon the efficiency by which ice crystals form and fall out of rising air parcels. *Jensen and Pfister* [2004] used a microphysical dynamical model to calculate freeze-drying of air that is slowly rising across the tropical tropopause.

[3] *Corti et al.* [2006] emphasize that deep convection of moderate strength transports tropical air to the maximum outflow altitude of 13 km, corresponding to a potential temperature ($\theta$) of 350 K. Figure 5 of *Corti et al.* [2006] illustrates that gaseous radiative heating lifts air from the level of clear sky radiative heating at 360 K (15 km) to, and above, the cold point tropopause near 380 K ($\sim$17 km). There is therefore a need to bridge a dynamical gap of several kilometers from 13 to 15 km altitude. "Cloud lofting," by which infrared absorption in thin high cirrus results in enhanced heating rates below the tropical tropopause and enhanced upward transport, is proposed to provide the key missing dynamical element for understanding transport in the upper troposphere/lower stratosphere (UT/LS). As discussed by *Corti et al.* [2005], air inside thin high clouds, without underlying optically thick clouds, is heated due to infrared absorption. In the zonal average this in situ heating dominates the cooling from underlying clouds, leading to a lower level of zero net radiative heating by 0.5–1 km.

[4] Though this paper focuses upon observations of tropical cirrus by satellite experiments, cirrus is of interest on the global scale. *Sassen* [2002] reviews the capabilities and limitations of current cirrus research, the different optical depth ranges of cirrus, and the generating mechanisms of cirrus. *Lynch and Sassen* [2002] note that subvisual cirrus, which is a focus of this paper, is composed of small ice crystals of various shapes (long dimensions $<50$ $\mu$m), of small ice water content ($<2 \times 10^{-4}$ g/m$^3$) and is located in clouds with $<1$ km vertical depths and horizontal scales from 20 to 2000 km.

[5] Observations of cirrus in the upper troposphere have been made by a variety of satellite instruments. *Wang et al.* [1996] compiled a 6 year climatology, from 1985 to 1990, of cloud occurrence frequency using Stratospheric Aerosol and Gas Experiment (SAGE) II limb-view extinction measurements. Extinctions measured between the low and high extinction limits for SAGE II of $2 \times 10^{-4}$ km$^{-1}$ and $2 \times$

[1]Atmospheric Chemistry Division, National Center for Atmospheric Research, Boulder, Colorado, USA.
[2]Center for Limb Atmospheric Sounding, University of Colorado at Boulder, Boulder, Colorado, USA.
[3]Department of Atmospheric, Oceanic and Planetary Physics, Oxford University, Oxford, UK.
[4]Jet Propulsion Laboratory, California Institute of Technology, Pasadena, California, USA.
[5]NASA Langley Research Center, Hampton, Virginia, USA.


0148-0227/10/2009JD012100$09.00

$10^{-2}$ $km^{-1}$ correspond mainly to subvisual cirrus. Clouds with extinctions greater than $2 \times 10^{-2}$ $km^{-1}$ produced solar occultation transmittances that precluded extinction retrievals, and are categorized as opaque clouds. *Wang et al.* [1996] presents zonal cross sections and longitude-latitude maps at several altitudes of subvisual and opaque clouds. Zonal maps of subvisual cirrus show a multilobed distribution of cloud frequency, with maximum in the tropics between 12 and 16 km altitude, midlatitude maxima at latitudes northward of 35°N, and minima between 20°–30°N and 25°S–35°S. Enhanced cloud frequency is apparent over the Maritime continent (Indonesia), Africa, and South America, with clouds present up to approximately 18.5 km altitude. At 17.5 km altitude cloud frequency is usually largest over the equator, except for June-July-August, months associated with the Indian summer monsoon, when clouds are present over Northern India and southern Tibet.

[6] Limb-view observations of cirrus at 12 $\mu$m by the Cryogenic Limb Array Etalon Spectrometer (CLAES) [*Mergenthaler et al.*, 1999] revealed geospatial distributions of subvisual cirrus similar to the SAGE II observations, with maxima over the Maritime continent, Africa, and South America. The CLAES data revealed an eastward shift in extinction associated with the 1992 El Niño, which shifted deep convection eastward. Fewer cirrus were observed at the 68 hPa level in the winter of 1991–1992 compared to 1992–1993, possibly due to the effects of the Mount Pinatubo volcano. A cloud extinction threshold (lower limit) of $9.0 \times 10^{-4}$ $km^{-1}$ was adopted by *Mergenthaler et al.* [1999] to distinguish clouds from aerosol. We will adopt this extinction threshold in our analyses of the HIRDLS 12 $\mu$m extinction data. Extinctions up to $4 \times 10^{-3}$ $km^{-1}$ usually had error estimates less than 30%, the error estimate cutoff chosen by *Mergenthaler et al.* [1999].

[7] A precursor to the CALIPSO experiment, the Lidar In-space Technology Experiment (LITE), measured cloud structure during September 10–19 1994 during a 10-day Space Shuttle mission [*Winker and Trepte*, 1998; *Omar and Gardner*, 2001]. "Laminar" cirrus, with vertical depths between a few hundred meters to one kilometer, and horizontal scales up to 2700 km, were observed between 35°N and 20°S at altitudes greater than 15 km approximately 7% of the time. Mean cloud depths and horizontal lengths of the laminar cirrus were 0.47 km and 500 km, respectively, at a mean altitude of 16.3 km.

[8] *Dessler et al.* [2006a] analyzed the distribution of optically thin cirrus in the tropics near the tropopause (i.e., $\theta$ from 360 to 400 K, altitudes from 13.7 to 16.2 km) using Geoscience Laser Altimeter System (GLAS) data for 29 September through 17 November 2003. Near-tropopause cirrus was 2 to 6 times more frequent over deep convection than over the equatorial western Pacific "cold pool," a climatological temperature minimum that is thought to be associated with parcel dehydration processing. The locations of the occurrence maxima in morning and evening were very similar. GLAS frequencies of occurrence of cirrus were larger in the evening than in the morning, and observed more frequently over land than ocean [*Dessler et al.*, 2006b]. *Wang and Dessler* [2006] used GLAS data for the same time period to calculate cloud overlap statistics. Clouds were detected 75.1% of the time in the tropics, with single-layer and multilayer clouds occurring 46.5 and 28.6% of the time, respectively.

[9] With the assemblage of the NASA A-train complement of satellites, it is possible to extend the studies discussed above. The Cloud-Aerosol Lidar with Orthogonal Polarization (CALIOP) lidar of the CALIPSO experiment [*Winker et al.*, 2007; *Vaughan et al.*, 2004] has measured cloud backscatter from June 2006 to the present. The HIRDLS experiment has archived cloud extinction from January 2005 through December 2007. In this paper we focus upon data for 1 year, from September 2006 through August 2007. Our main goal is to present calculations of the spatial and temporal distributions of cirrus in the upper troposphere as observed by the HIRDLS and CALIPSO experiments. These distributions and associated statistics will be useful in validation studies of three-dimensional models that simulate cirrus structure.

[10] In section 2 we discuss the various data sets used in this paper. The similarities of the geospatial patterns of the *Wang et al.* [1996], HIRDLS, and CALIPSO seasonal cloud frequencies are presented in section 3. Monthly averages of HIRDLS and CALIPSO cloud occurrence frequencies are intercompared with Microwave Limb Sounder (MLS) relative humidity with respect to ice (RHI) data in section 4. As expected from microphysical considerations, there is a clear similarity between the three data sets. CALIPSO horizontal and vertical scales are discussed in section 5. These scales are of interest from both observational and physical perspectives. Though CALIPSO uses a nadir-viewing geometry, and HIRDLS uses a limb-viewing geometry, the large horizontal scales of the cirrus observed by the CALIPSO experiment produces the situation that geospatial distributions of cirrus are similar for the two experiments. The identification of the location and occurrence frequency of laminar cirrus is of interest since the accurate specification of laminar cirrus in global models is important for the accurate simulation of lower stratospheric dehydration, and also of interest due to the potential of cloud lofting to influence vertical transport. In section 6 we relate the normalized distributions of cirrus and opaque tropical clouds to Climate Diagnostic Center (CDC) outgoing longwave radiation (OLR), a proxy for deep convection. These time-averaged distribution functions can be compared to the statistical distributions of the cloud structure as calculated by models.

## 2. Data

[11] The HIRDLS experiment was designed to measure chemical species mixing ratios, and cloud and aerosol extinction. Instrumental Kapton plastic, however, became loose after launch, obstructs the field of view, and overlies the moving scan mirror. This obstruction introduces a complicated time-varying signal to all of the 21 filter channels. Hard work has characterized this signal, leading to Version 4 retrievals of temperature, $O_3$, $HNO_3$, CFC-11, CFC-12, and 12 $\mu$m extinction profiles [*Gille et al.*, 2008; *Kinnison et al.*, 2008; *Nardi et al.*, 2008; *Massie et al.*, 2007]. The retrieval methodology is discussed by *Khosravi et al.* [2009]. With a vertical resolution of 1 km, and an along-track repeat cycle every 110 km, there are approximately 5500 profiles measured each day. The precisions of

the various measurements are discussed in the Data Description and Quality document, available at http://www.eos.ucar.edu/hirdls/.

[12] HIRDLS radiances are greatly enhanced in the 12 $\mu$m channel when clouds are present along tangent raypaths. Archived data (available at http://disc.sci.gsfc.nasa.gov/data/data pool/HIRDLS/index.html) specifies cloud flags and extinctions specified in a pressure grid, and cloud top pressures. Pressure levels between 83 and 177 hPa, in 10% pressure steps, are the primary focus in this paper. The cloud flags are calculated by computer routines that examine the structural details of radiance profiles, and indicate the pressure levels at which radiance perturbations are larger than clear sky radiances. Cloud flag values of 0, 1, 2, 3, and 4 denote clear sky, unknown cloud type, cirrus layers, polar stratospheric clouds, and opaque clouds. Cloud flags are determined before the extinction profile is retrieved (see *Massie et al.* [2007] for a full description of the cloud identification methodology). Figure 1 of *Massie et al.* [2007] displays examples of the various types of radiance profiles, due to different cloud types, that are observed by HIRDLS. Opaque clouds have a radiance profile in which the radiance saturates (i.e., radiances are constant with altitude below the cloud top). The operational retrieval does not retrieve meaningful extinction values for opaque clouds. The unknown cloud type has a variety of radiance perturbations in the radiance profile, and is likely produced by a variety of clouds along the raypath. The unknown cloud type includes situations in which a cirrus layer is located over a many kilometer deep cloud structure. The cirrus layer radiance profile has a narrow radiance maximum at the altitude of the cirrus layer. These radiance signatures correspond to laminar cirrus (of small vertical depth) that is isolated from other cloud structure. Clear-sky radiance profiles do not have radiance perturbations that are larger than radiance profile noise variations.

[13] Improvements in the retrieval algorithm, subsequent to the retrieval discussed by *Massie et al.* [2007], has produced Version 4 12 $\mu$m extinction values between 20 and 215 hPa in the range of extinction from $10^{-5}$ to $10^{-2}$ km$^{-1}$. Since the 12 $\mu$m extinctions are unique, with no other 12 $\mu$m extinctions currently available, validation of the HIRDLS extinction requires comparisons to previous data. Using the cloud extinction threshold of $9.0 \times 10^{-4}$ km$^{-1}$ of *Mergenthaler et al.* [1999], HIRDLS 100 hPa zonal averages of tropical cloud extinction are biased high approximately by a factor of 1.4 compared to the CLAES zonal averages.

[14] CALIPSO CLay files (available at http://eosweb.larc.nasa.gov/PRODOCS/calipso/table_calipso.html) are used to calculate cloud frequency of occurrence, and vertical and horizontal scales in the upper troposphere. The CAL_LID_L2_05kmCLay-Prov-V1-20 files specify the cloud tops and bases (in kilometers) of clouds along the orbital track. These files have a 5 km horizontal resolution for the full column. The cloud feature and layer properties algorithms are discussed by *Vaughan et al.* [2005]. Cloud/aerosol discrimination is achieved by application of an adaptive threshold on the magnitude and variation of the lidar backscatter at both wavelengths (532 and 1064 nm) [*Liu et al.*, 2004; *Vaughan et al.*, 2004]. In comparisons of CALIPSO and ground based lidar measurements, observed using the same two lidar wavelengths as the CALIOP lidar, *Kim et al.* [2008] determined that cloud top and base heights of the two lidars agreed to within 0.10 km.

[15] MLS RHI [*Read et al.*, 2007] data (available at http://mirador.gsfc.nasa.gov/cgi-bin/mirador/presentNavigation.pl?tree = project) are archived at 83, 100, 121, 147, 178, 215, 261, and 336 hPa. There are approximately 4000 profiles per day. RHi is computed from the standard products of water and temperature using the Goff-Gratch [*List*, 1951] ice humidity saturation formula, and is measured in the presence of clouds. The vertical resolutions of the RHI measurements vary between 4 and 6 km between 83 and 316 hPa, with RHI precisions between 1 and 14% in RHI units, and accuracies between 20 and 35%. Further information on the Version 2.2 level 2 RHI data is included in the MLS Data Quality Document (see http://mls.jpl.nasa.gov/data/datadocs.php).

[16] While HIRDLS, CALIPSO, and MLS are in the A-train, their observational geometries are quite different. The HIRDLS line of sight is oriented 47° to the anti-Sun side of the orbital plane, looking backward. MLS looks forward along the orbital track, with a tangent point in front of the AURA spacecraft, while CALIPSO observes in the nadir direction. The three instruments therefore observe different volumes of the atmosphere, precluding direct comparisons of the daily data.

[17] Since the limb geometry integrates over a several hundred kilometer path centered at the tangent ray point, the limb-view extinction differs from a hypothetical nadir-view extinction measurement. One can encounter a tangent raypath for which clouds are detected in the limb view, while the nadir view sees no clouds. Two thirds of the observed radiance originates along a 150 km ray segment, centered at the tangent point of the limb-view raypath, for a cirrus layer of 1 km vertical depth. For situations in which the horizontal distribution of cloud optical depth is uniform over approximately 150 km, the nadir and limb-view geometries will produce similar cloud frequencies. The observed CALIPSO horizontal cloud scales are discussed in section 5. Finally, MLS and HIRDLS measurements are observed with different vertical resolutions, and are reported on pressure grids, while the CALIPSO data is reported on an altitude scale. Some differences in the three data sets are expected due to these considerations.

[18] Climate Diagnostic Center (CDC) OLR data [*Liebmann and Smith*, 1996] (available at http://www.cdc.noaa.gov) are used in this study to relate daily locations of deep convection to HIRDLS and CALIPSO data. OLR less than 170 W m$^{-2}$ (which correspond to a brightness temperature of 235°K) indicates the location of very deep convection. A deep convective cloud system will have a cloud top at a high altitude and emit less radiation (due to the cold cloud top temperature) than a cloud system at a lower altitude (and higher cloud top temperature). The CDC data are specified daily at every 2.5° in latitude and longitude.

## 3. Seasonal Variations

[19] HIRDLS and CALIPSO seasonal variations of cloud frequency of occurrence at 121 hPa (~15 km) and 90 hPa

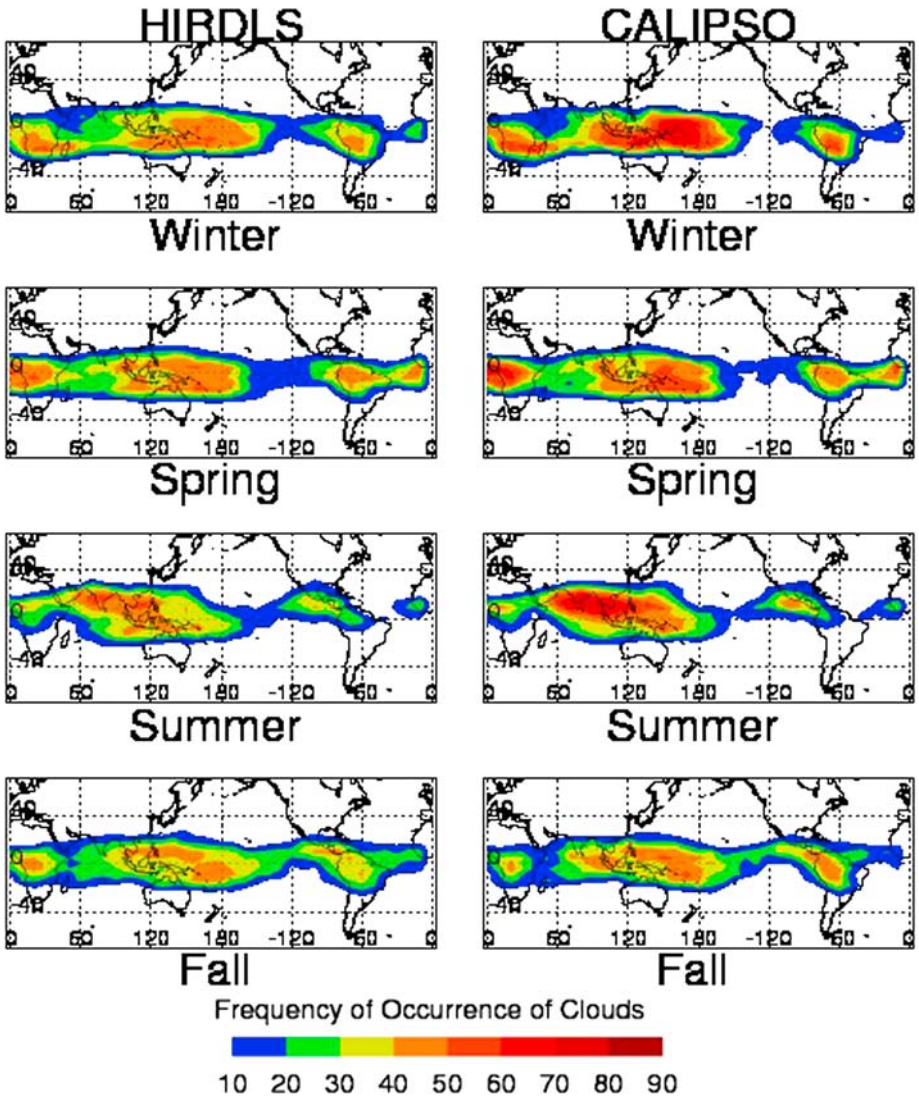


**Figure 1.** Seasonal variations of cloud frequency of occurrence at 121 hPa and 15 km. Opaque clouds are not included in the calculation of these frequencies.

(~17 km) are displayed in Figures 1 and 2. Cloud frequency is binned in 10° longitude by 5° latitude bins. Maxima are present over the Maritime continent, South America, and Africa with minima near 120°W and 60°E. Figures 1 and 2 are similar to the cloud frequency patterns of *Wang et al.* [1996, Plate 4]. Seasonal variations in cloud occurrence show a clear modulation by the Indian monsoon. Cloud frequency moves northward to a location over India and southern Tibet during the summer.

[20] CALIPSO cloud frequencies in Figures 1 and 2 are calculated by determining the fraction of the time that a cloud is present in an altitude grid with 1 km vertical spacing. This calculation is done for each longitude-latitude grid box. The CLay files specify the altitude ranges for which clouds are present along the orbital track. If an altitude range specifies the presence of clouds between, for example, 16.2 and 18.5 km, then clouds are specified to be present in the altitude ranges 16–17, 17–18, and 18–19 km altitude at that observation point. Since two CLay cloud ranges could be in the 17 to 18 km altitude (e.g., a cloud top could be at 17.2 km and a cloud bottom at 17.6) care is taken not to double count cloud frequency in the 17 to 18 km altitude range.

[21] All HIRDLS observations for which clouds are flagged, and for which extinctions are between $9.0 \times 10^{-4}$ and $1.0 \times 10^{-2}$ $km^{-1}$, are used to determine the cloud frequencies in Figures 1 and 2. *Wang et al.* [1996] comments that SAGE II opaque clouds are detected by noting where the SAGE retrieval cuts off due to low transmittances (high cloud opacity). For HIRDLS, opaque clouds are identified from examination of the vertical shape of the radiance profile. An opaque cloud has very large optical depth along the raypath, and the retrieval will not report extinction below the cloud top. Thus, Plate 4 of *Wang et al.* [1996] and Figures 1 and 2 present cloud frequencies for subvisual cirrus (i.e., opaque clouds are not included).

[22] The 90 hPa pressure level is displayed in Figure 2 to illustrate how the cirrus occurrence frequency precipitously decreases as the tropopause is encountered. *Fu et al.* [2007] calculated cloud fractions using CALIPSO data from June

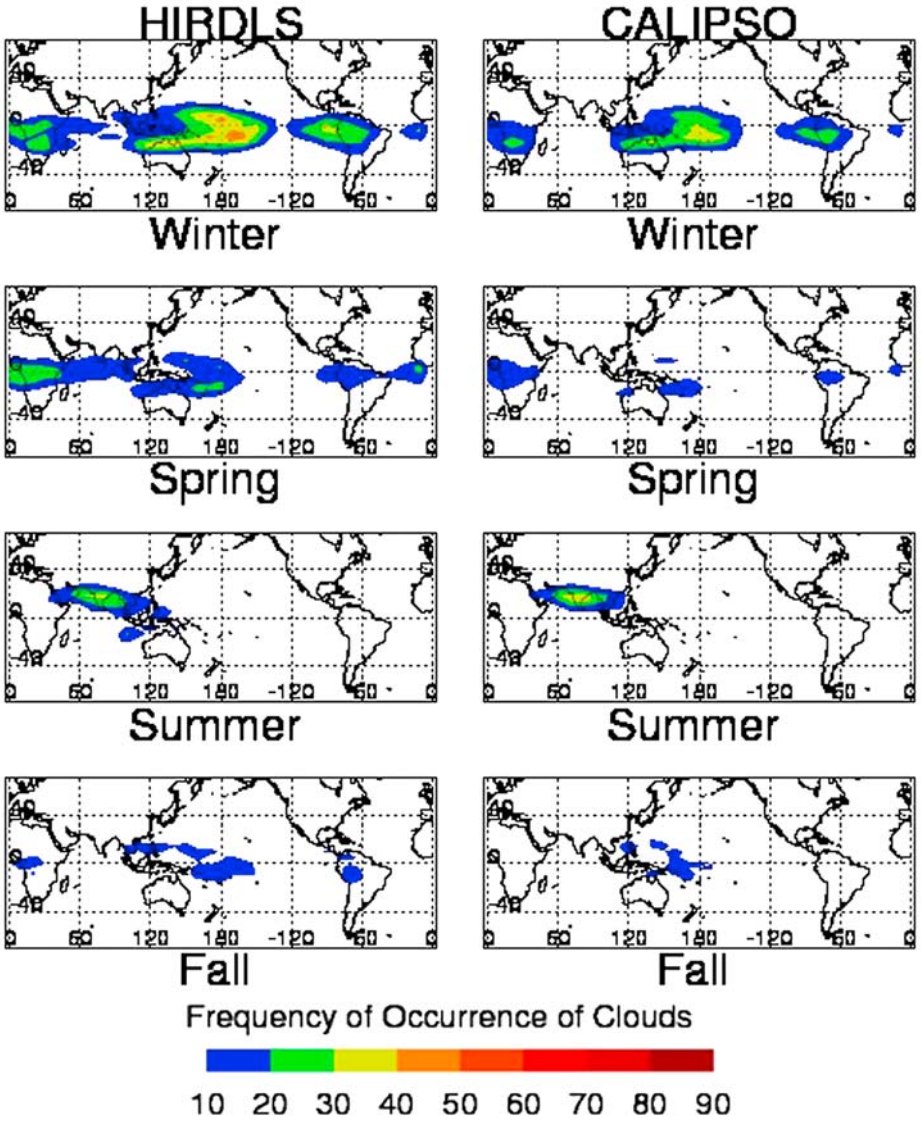


**Figure 2.** Seasonal variation of cloud frequency of occurrence at 90 hPa and 17 km. Opaque clouds are not included in the calculation of these frequencies.

2006 to September 2007. The total cloud fractions between 20°S and 20°N are about 0.05% at 18.5 km, 0.5% at 18.0 km and 5% at 17.0 km [see *Fu et al.*, 2007, Figure 2].

[23] Since SAGE and HIRDLS measured extinction at 1.02 and 12 $\mu$m, respectively, it is of interest to comment on the expected differences in the cloud frequencies due to the differences in the observational wavelengths and sensed cloud optical depths. Using the subvisible cirrus measurements of *Lawson et al.* [2008], measured over Central America by in situ particle size experiments on the NASA WB-57 in January–February of 2006, Mie calculations of extinction at the two wavelengths differ by 4%. The *Lawson et al.* [2008] size distribution has a mean radius of 8.8 $\mu$m. Thus, similar optical depths are probed by the two limb-viewing experiments.

[24] Figure 3 displays seasonal variations of isolated cirrus frequency at 121 hPa and 15 km, when CALIPSO cirrus vertical depths are 1 km or less. An example of isolated cirrus is given in Plate 1 of *Winker and Trepte* [1998] in which no clouds are present below a cloud near ~17 km altitude with a ~1 km vertical depth and horizontal length of ~660 km. HIRDLS observations for which isolated cirrus layers are flagged (i.e., the cloud flag is equal to 2) and for which extinctions are between $9.0 \times 10^{-4}$ and $1.0 \times 10^{-2}$ km$^{-1}$ are used to determine the cloud frequencies in Figure 3. Figure 3 therefore indicates where isolated laminar cirrus is located for each season. Figure 1 includes a variety of cloudy situations, while Figure 3 is restricted to isolated cirrus. The paucity of isolated cirrus over the maritime continent in Figure 3 is discussed later in this section, in relation to the location of deep convection.

[25] Tables 1 and 2 present CALIPSO occurrence frequencies of isolated laminar cirrus for all longitudes for the tropics (20°S–20°N) and for the maritime continent (100°E–140°E). The altitudes in Tables 1 and 2 are altitudes of the cloud tops. Averages are presented as a function of the vertical depths of the cirrus (i.e., the vertical depth ranges of [0.2, 1], [0.2, 2], and [0.2, 3], in km). Maximum

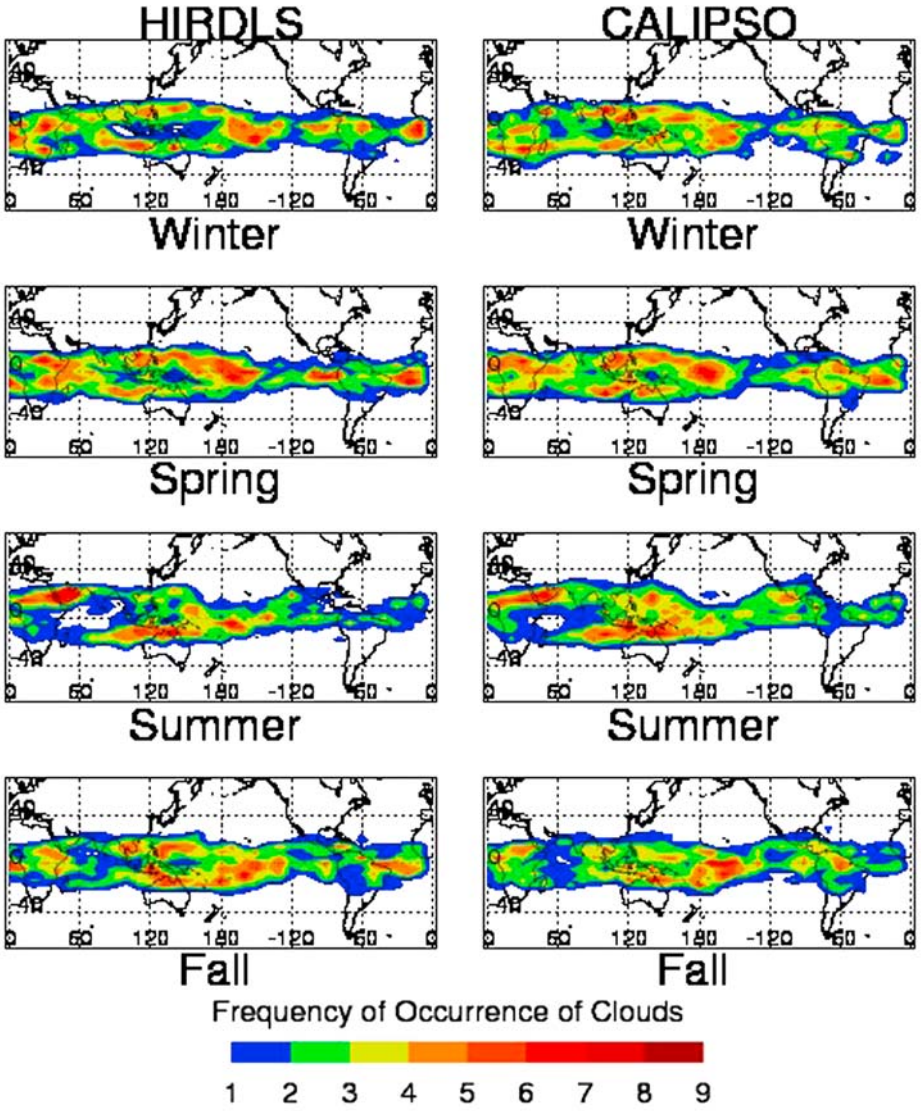


**Figure 3.** Seasonal variations of isolated cirrus frequency of occurrence at 121 hPa and 15 km. CALIPSO cirrus vertical depths are 1 km or less. HIRDLS cirrus layers (i.e., the cloud flag is equal to 2) were counted in preparing the graph. Cirrus layers are present away from the maritime continent (where deep convection is present).

frequencies are the largest frequencies observed in the longitude-latitude grid boxes of the mapped data. Clouds were identified as isolated laminar cirrus if there was a clear sky region greater than 5 km below the base of the cirrus. The frequencies of occurrence at 15 and 16 km altitude vary between 3 and 12% as the vertical depth increases. In general, laminar cirrus occurs much less frequently than total cloud frequency, which is approximately 33% over the maritime continent (i.e., the average of the 28.3 and 38.9% frequencies at 15 and 16 km altitude in Table 2). The low laminar frequencies observed by CALIPSO and HIRDLS

**Table 1.** CALIPSO Cloud Frequency of Occurrence in Winter for All Longitudes Between 20°S and 20°N[a]

| | Average (%) | | | | Maximum (%) | | | |
|---|---|---|---|---|---|---|---|---|
| Altitude (km) | D < 1 km | D < 2 km | D < 3 km | All | D < 1 km | D < 2 km | D < 3 km | All |
| 16 | 2.9 | 6.1 | 7.5 | 19.0 | 11.2 | 25.0 | 32.2 | 68.5 |
| 15 | 2.4 | 6.3 | 8.6 | 24.0 | 7.9 | 18.4 | 26.1 | 80.9 |

[a]Winter is December, January, and February. D is the vertical depth of the isolated laminar cirrus (with a clear region >5 km below the cirrus base). "All" values count all types of clouds.

**Table 2.** CALIPSO Cloud Frequency of Occurrence in Winter for the Maritime Continent Between 20°S and 20°N[a]

| | Average (%) | | | | Maximum (%) | | | |
|---|---|---|---|---|---|---|---|---|
| Altitude (km) | D < 1 km | D < 2 km | D < 3 km | All | D < 1 km | D < 2 km | D < 3 km | All |
| 16 | 3.3 | 7.2 | 9.4 | 28.3 | 11.2 | 25.0 | 32.2 | 68.5 |
| 15 | 3.4 | 8.6 | 12.1 | 38.9 | 7.9 | 18.4 | 26.1 | 80.9 |

[a]Winter is December, January, and February. Maritime continent is 100°E–140°E. D is the vertical depth of the isolated laminar cirrus (with a clear region > 5 km below the cirrus base). "All" values count all types of clouds.

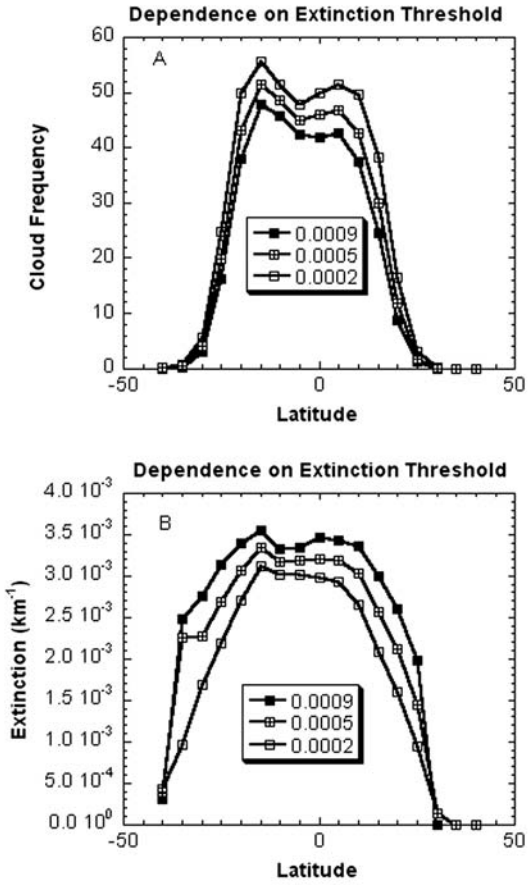


**Figure 4.** (a) Sensitivity of HIRDLS cloud frequency (during winter at 121 hPa) to the lower extinction threshold (in $km^{-1}$). Averages are calculated for the range from 100°E to 140°E longitude. (b) Sensitivity of the HIRDLS zonal average of extinction to the applied lower extinction threshold.

are similar to the 7% LITE value reported by *Winker and Trepte* [1998]. Section 5 examines the distributions of cirrus depths and horizontal scales in more detail.

[26] Figure 4 illustrates the sensitivity of the cloud frequency of occurrence and zonal extinction averages to choice of the cloud extinction threshold. It is useful to quantify this sensitivity because there are clouds present in which the extinction is less than the threshold value of 0.0009 $km^{-1}$. HIRDLS zonal averages of cloud frequency and extinction over the maritime continent (100°E–140°E) during 2005–2007 were calculated for the $km^{-1}$ extinction ranges [0.0002, 0.01], [0.0005, 0.01], and [0.0009, 0.01] for each season to quantify this sensitivity. Figures 4a and 4b are for the winter season (December–February) and present averages calculated for the three extinction ranges. The cloud frequency and extinction curves exhibit a modest sensitivity of 15% to the cloud extinction threshold.

[27] Figure 5 presents the geospatial relationship between deep convection and isolated laminar cirrus, identified by noting when the HIRDLS cloud flag is equal to 2. Figure 5a presents the frequency of occurrence of laminar cirrus at 121 hPa in relation to the frequency of occurrence of deep convection (i.e., when OLR is less than 170 $W/m^2$). Laminar cirrus is concentrated away from the equator (see Figure 3), while deep convection is most prevalent near 10°S. This is reinforced in Figure 5b, which presents average OLR during winter. Lowest OLR is concentrated between the equator and 10°S. This geospatial relationship is a result of the fact that low OLR values are associated with cloud structure that extends throughout a range of altitude and/or is multilayered. This cloud structure has cloud radiance perturbations throughout a range of altitude, while the isolated cirrus layer radiance perturbations are localized at the height of the cirrus layer.

[28] Laminar cirrus also can be located over vertically extensive cloud structure. Plate 3 of *Winker and Trepte* [1998] displays an example of this situation in which laminar cirrus at ~18 km altitude is separated from a lower cloud structure that is present between 8 and 16 km altitude. Table 3 presents CALIPSO cloud occurrence frequencies for cases in which laminar cirrus has a vertical depth less than 2 km, is separated vertically from a lower cloud by more than 1 km, and the vertical depth of the lower cloud structure is greater than 4 km. Occurrence frequencies, on

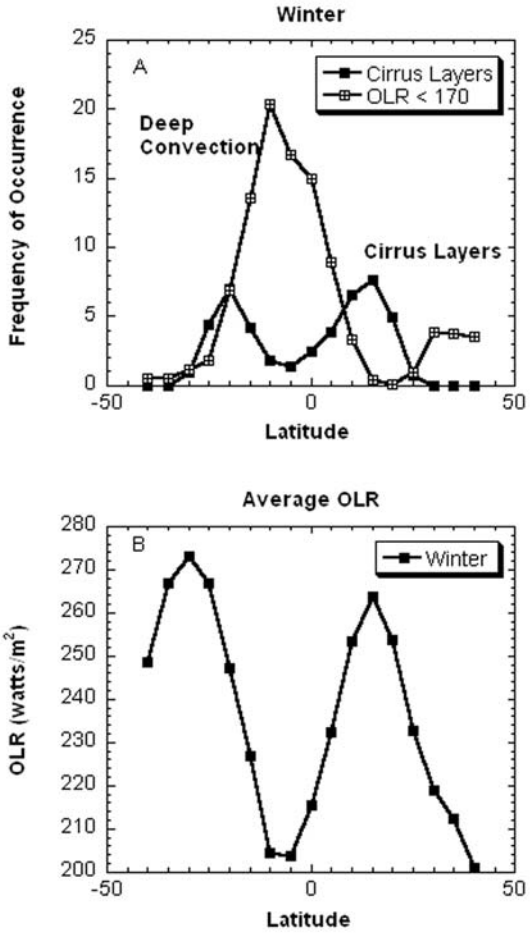


**Figure 5.** (a) The frequency of occurrence of isolated laminar cirrus at 121 hPa in relation to deep convection (OLR less than 170 $W/m^2$). Isolated cirrus layers are concentrated away from the equator (i.e., away from deep convection). (b) Average OLR during winter has lowest OLR concentrated between the equator and 10°S.

**Table 3.** CALIPSO Cloud Frequency of Occurrence in Winter, When Laminar Cirrus is Over Thicker Clouds, for All Longitudes and for the Maritime Continent Between 20°S and 20°N[a]

| | All Longitudes (%) | | Maritime Continent (%) | |
|---|---|---|---|---|
| Altitude (km) | Average | Maximum | Average | Maximum |
| 16 | 0.16 | 1.9 | 0.17 | 1.9 |
| 15 | 0.13 | 2.0 | 0.14 | 2.0 |

[a]Winter is December, January, and February. Maritime continent is 100°E–140°E. The topmost cloud is laminar cirrus with a depth less than 2 km. The vertical separation of the first and second clouds is greater than 1 km in altitude. The lower cloud has a depth greater than 4 km.

average, are on the order of 0.15% for all longitudes and for the maritime continent (100°E–140°E) between 20°S and 20°N.

## 4. Monthly Observations of Cirrus

[29] Figures 6 and 7 display monthly averages of HIRDLS and CALIPSO cloud occurrence frequencies at 161 hPa and 13 km, respectively, for April and June 2007 and MLS RHI at 177 hPa (the nearest MLS pressure level). Data from these 2 months are shown to demonstrate representative differences in monthly averages, and to demonstrate how the cloud frequency relates to MLS RHI. It is apparent that the geospatial patterns of cloud frequency are similar for the HIRDLS and CALIPSO experiments, and correlated to the geospatial patterns of MLS RHI.

[30] It is readily apparent that there are regions in which average MLS RHI is less than 100% and yet the average cloud occurrence is large. Clouds do not persist at RHI less than 100%. The physical contradiction between the quantitative values of RHI and cloud occurrence is likely due to the fact that the MLS vertical field of view is ~5 km, while laminar cirrus is typically a kilometer in vertical depth. Situations may arise in which RHI is less than 100% in a 5 km vertical path, while greater than 100% in a vertically narrow cloud structure, yielding a vertically average RHI less than 100%.

[31] Figure 8 presents the colocated 5° latitude × 10° longitude RHI and CALIPSO cloud frequency monthly

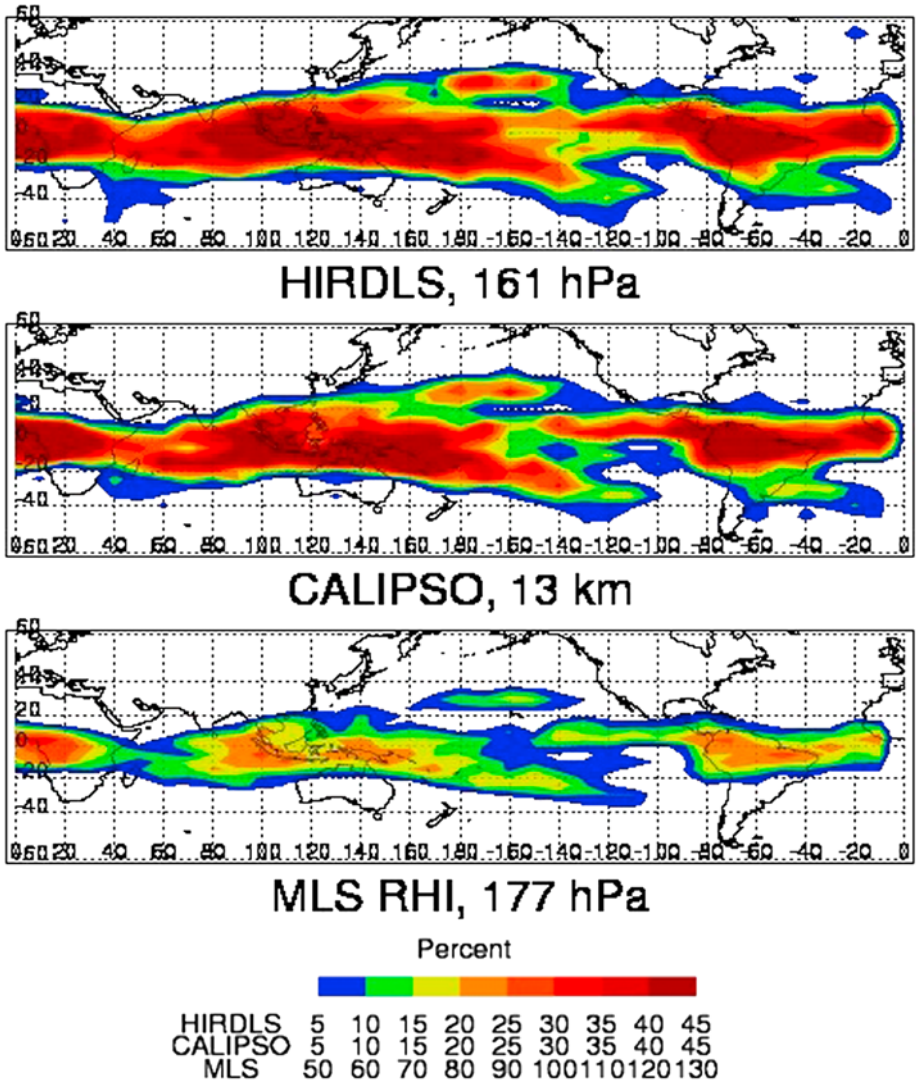


**Figure 6.** HIRDLS and CALIPSO cloud frequency of occurrence at 161 hPa and 13 km during April 2007 and MLS RHI at 177 hPa.

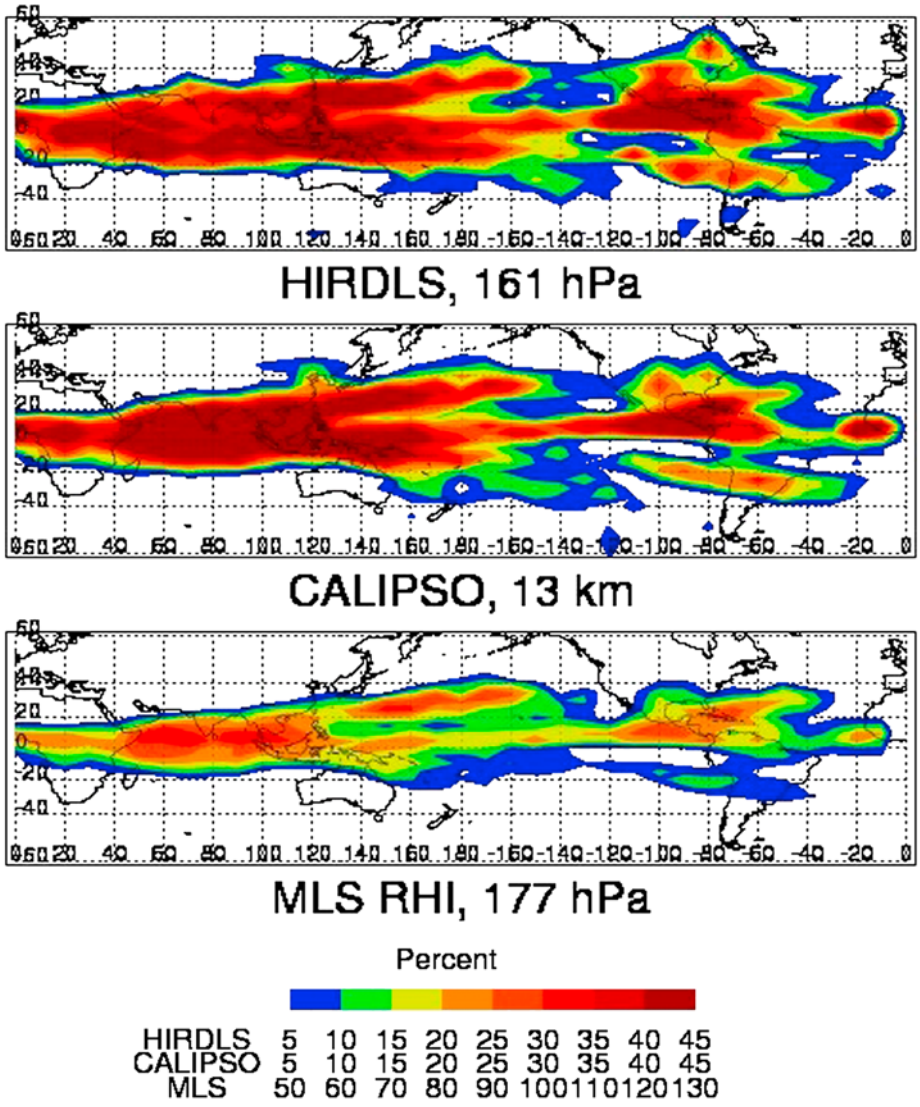


**Figure 7.** HIRDLS and CALIPSO cloud frequency of occurrence at 161 hPa and 13 km during June 2007 and MLS RHI at 177 hPa.

averages, used to prepare Figure 7. Only a few data pairs have RHI values greater than 100%. The two sets of RHI–cloud frequency pairs, however, correlate well (with a correlation coefficient of 0.88).

[32] Figure 9 presents the monthly variations of all clouds near 100 hPa for 20°S–20°N. Averages were calculated for the cloud frequency range between 5 and 100%. Note that the time series has a temporal break for August 2007, followed by September 2006, as marked by the vertical line. The selection of months was chosen to include continuous months during winter (December-January-February, DJF) since largest cloud frequencies are present during winter. *Mergenthaler et al.* [1999] noticed that CLAES cloud frequencies at 68 and 100 hPa were lowest during June–August 1992–1993. *Comstock et al.* [2002] also observed that there was a noticeable decrease in high-altitude cirrus, as measured by the Micropulse Lidar at Nauru (0.5°S, 166.9°E) in 1999. *Massie et al.* [2003] calculated cloud occurrence averages using Halogen Occultation Experiment (HALOE) extinction at 121 hPa for

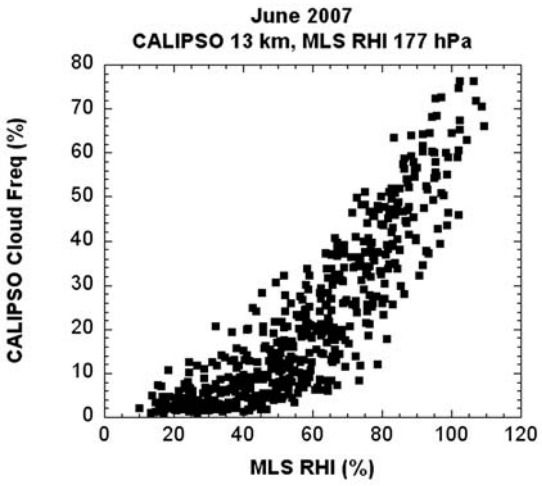


**Figure 8.** MLS RHI at 177 hPa and CALIPSO cloud frequency of occurrence at 13 km in June 2007.

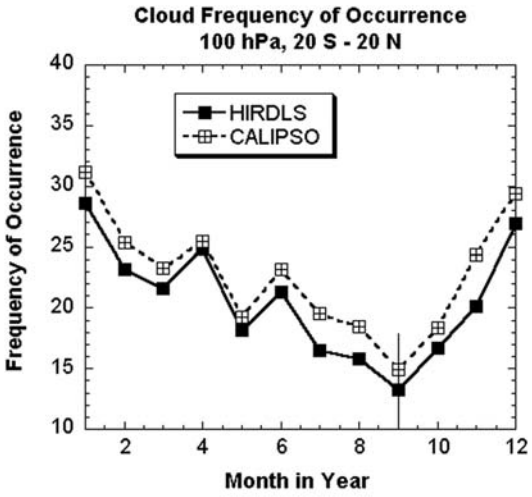


**Figure 9.** Monthly variations in all clouds at 100 hPa as observed by CALIPSO and HIRDLS for 20°S–20°N. Note that the time series has a temporal break for August 2007, followed by September 2006, as marked by the vertical line.

1993–1999 and Stratospheric Aerosol and Gas Experiment (SAGE II) extinction between 100 and 140 hPa for 1987–1999 in the tropics (20°S–20°N), and noted that the cloud frequencies were largest in winter, and smallest in summer. Warmer temperatures near the tropopause and less frequent deep convection both contributed to smaller values of extinction in summer. We also note that the zonal average transformed Eulerian mean (TEM) residual vertical velocity varies by a factor of 2 throughout the year in the tropics, with largest values in winter [*Randel et al.*, 2008]. The seasonality of Figure 9, and the seasonality of the zonal mean upwelling [see *Randel et al.*, 2008, Figure 2] are in phase with each other. Larger mean upwelling is expected to enhance cloud occurrence, since larger upwelling more readily replenishes water vapor that is needed to form cirrus.

## 5. Horizontal and Vertical Scales

[33] Figure 10 presents the locations, horizontal and vertical scales of cirrus observed by CALIPSO at 18 km. Cloud observations in January and February (days 1–59) are concentrated over the Maritime continent, Africa, and South America (see Figure 1). In June and July (days 150–200) there is a notable concentration of (monsoon related) cirrus over India. There is a paucity of cirrus during August and September (days 213–273). Largest horizontal lengths occur in winter and during summer.

[34] The horizontal scales in Figure 10 are calculated at each CLay data file observation point, which are separated by 5 km along the orbital track. CLay file cloud top data are first used to specify if a cloud is or is not present for altitudes between, for example, 18 and 19 km at each orbital track position. The continuous horizontal length is then calculated both in front of and in back of the orbital track observation point. This method is used to prepare the data

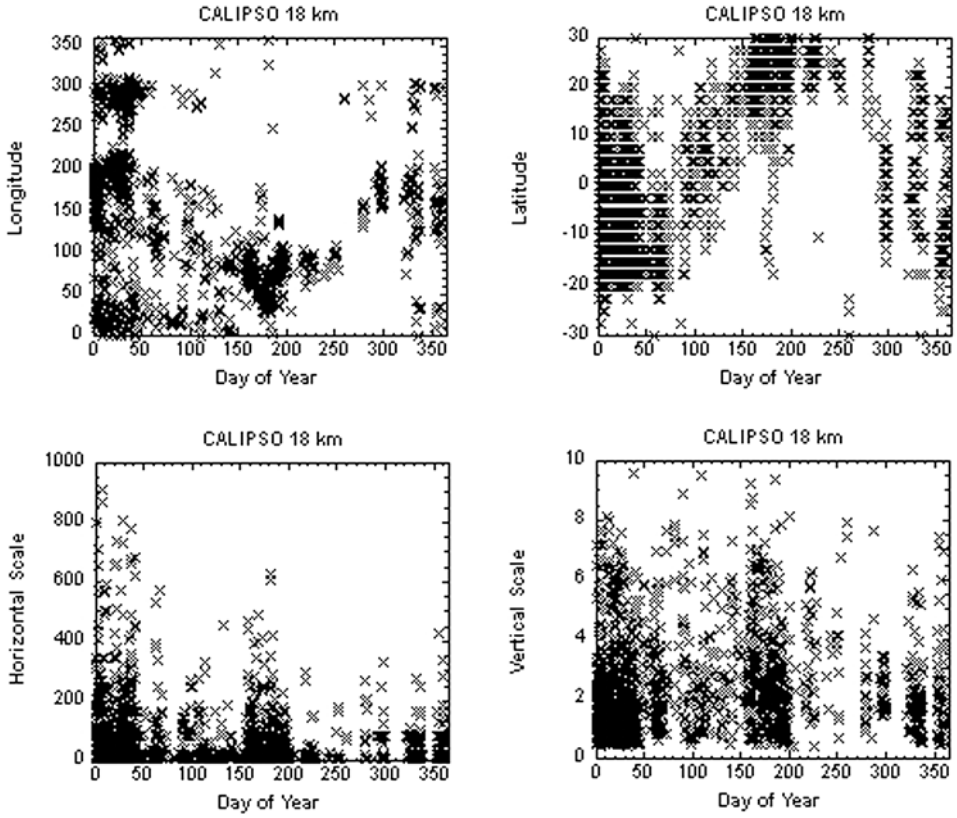


**Figure 10.** Locations and horizontal and vertical scales of cirrus observed by CALIPSO at 18 km altitude.

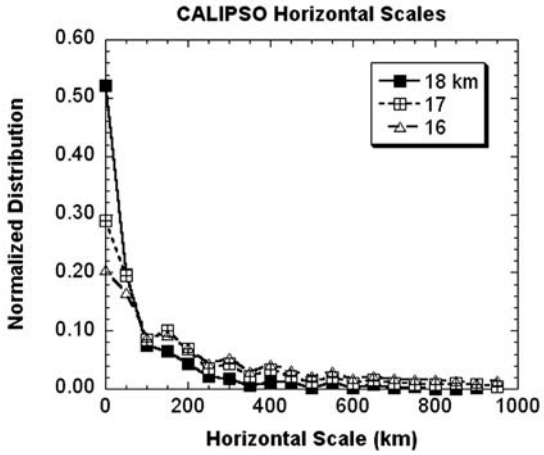


**Figure 11.** Continuous horizontal scales of cirrus as observed by CALIPSO at 16, 17, and 18 km (~100, 90, and 78 hPa, respectively).

featured in Figures 10, 11, 13, and 16. This method is pertinent to our discussions since it specifies the distribution of horizontal lengths that are present at each position along the orbital track, i.e., on a per meridional arc length basis.

[35] Statistics of the horizontal lengths were also calculated using a second method. Horizontal lengths were calculated along the orbital track by summing cloud-present continuous horizontal sequences of cloud tops in, for example, the 18 to 19 km altitude range. This counting of the cloud lengths determines cloud lengths on a per orbit basis and produces statistics that counts preferentially shorter lengths than longer lengths. Graphs using this second method are similar qualitatively to Figures 10, 11, 13, and 16 and are not shown.

[36] The vertical scales in Figures 10, 12, 13, and 15 are calculated using the CLay file cloud top and cloud bottom layer data. A cloud vertical scale is noted in Figure 10 if the cloud top is within, for example, the 18 to 19 km altitude range. The vertical depth of the cloud is the difference in the cloud top and cloud base altitudes.

[37] Figure 11 presents normalized distributions of the continuous CALIPSO horizontal scales at 16, 17, and 18 km altitude (~100, 90, and 78 hPa, respectively). The data were binned in increments of 50 km, with the first bin for the range between 5 and 50 km. Approximately half of the horizontal lengths occur for lengths greater than 100, 50, and 50 km at 16, 17, and 18 km, respectively. Though the CALIPSO and HIRDLS experiments use nadir and limb-view techniques, respectively, the large continuous horizontal scales of the cirrus observed by the CALIPSO experiment produces many situations in which the two experiments measure similar cloud frequencies. If the horizontal scales are predominantly small, then situations will arise in which the limb-viewing HIRDLS experiment will see clouds along the tangent raypath, while the nadir CALIPSO experiment will look along a clear-sky path.

[38] If the CALIPSO nadir and the HIRDLS limb tangent point sample volumes looked at the same volume of air, then we could count how many times the two instruments did/did not simultaneously count clouds, expressed as a function of the along-track CALIPSO horizontal length scale, and determine the range of horizontal scales for which the two experiments detect clouds in a similar manner. Unfortunately, CALIPSO looks in the nadir along its orbital track while the HIRDLS tangent point along the limb view is 3037 km away from the CALIPSO nadir point.

[39] Radiative transfer calculations indicate that whether or not the two experiments detect clouds in a similar manner is a function of both the cloud horizontal scale and the HIRDLS cloud extinction threshold. These calculations considered a single 1 km thick cloud with cloud extinction of $2 \times 10^{-3}$ km$^{-1}$ (see Figure 4) at 16 km altitude and cloud horizontal lengths between 20 and 300 km. The center of a single cloud is positioned in a random manner along the HIRDLS limb-view raypath at various distances from the CALIPSO nadir point. Cloud detection frequencies for both experiments were calculated for an ensemble of 100 cases per fixed cloud length. CALIPSO does not detect a cloud in the ensemble calculations if the cloud is not present along the nadir view. The average CALIPSO cloud detection frequency curve deviated from unity when the horizontal length scale is equal to or less than 70 km. The HIRDLS retrieval assumes that the cloud extinction is uniformly distributed along a spherical shell, so a short cloud length with extinction equal to $2 \times 10^{-3}$ km$^{-1}$ will yield a retrieved extinction less than $2 \times 10^{-3}$ km$^{-1}$. HIRDLS does not detect a cloud in the ensemble calculations if the retrieved extinction is less than the specified extinction threshold. Cloud detection frequencies for both experiments fell below 75% when the horizontal length scale decreased to 70 km for an extinction threshold of $8 \times 10^{-4}$ km$^{-1}$ (see Figure 4). If the extinction threshold is set to $5 \times 10^{-4}$ km$^{-1}$ then the HIRDLS detection frequency curve deviates from unity when the cloud length is 30 km. Thus, our assumed threshold of $9 \times 10^{-4}$ km$^{-1}$ leads to the situation that the HIRDLS and CALIPSO average cloud frequencies are similar because many cloud scales are greater than 70 km at 16 km (see discussion above in relation to Figure 11), and the HIRDLS and CALIPSO detection frequencies fall off in a roughly similar manner as cloud scales decrease below 70 km.

[40] Figure 12 presents normalized distributions of the CALIPSO vertical depths at 16, 17, and 18 km altitude. The data were binned in increments of 0.2 km, with the first bin

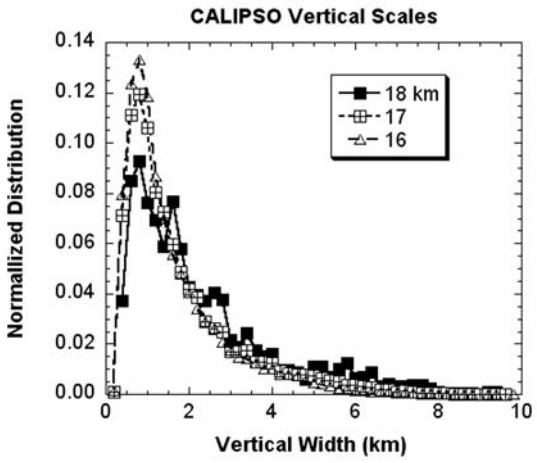


**Figure 12.** Vertical scales of cirrus as observed by CALIPSO at 17 km (~90 hPa) in the tropics. The pdfs peak between 0.8 and 1.0 km.

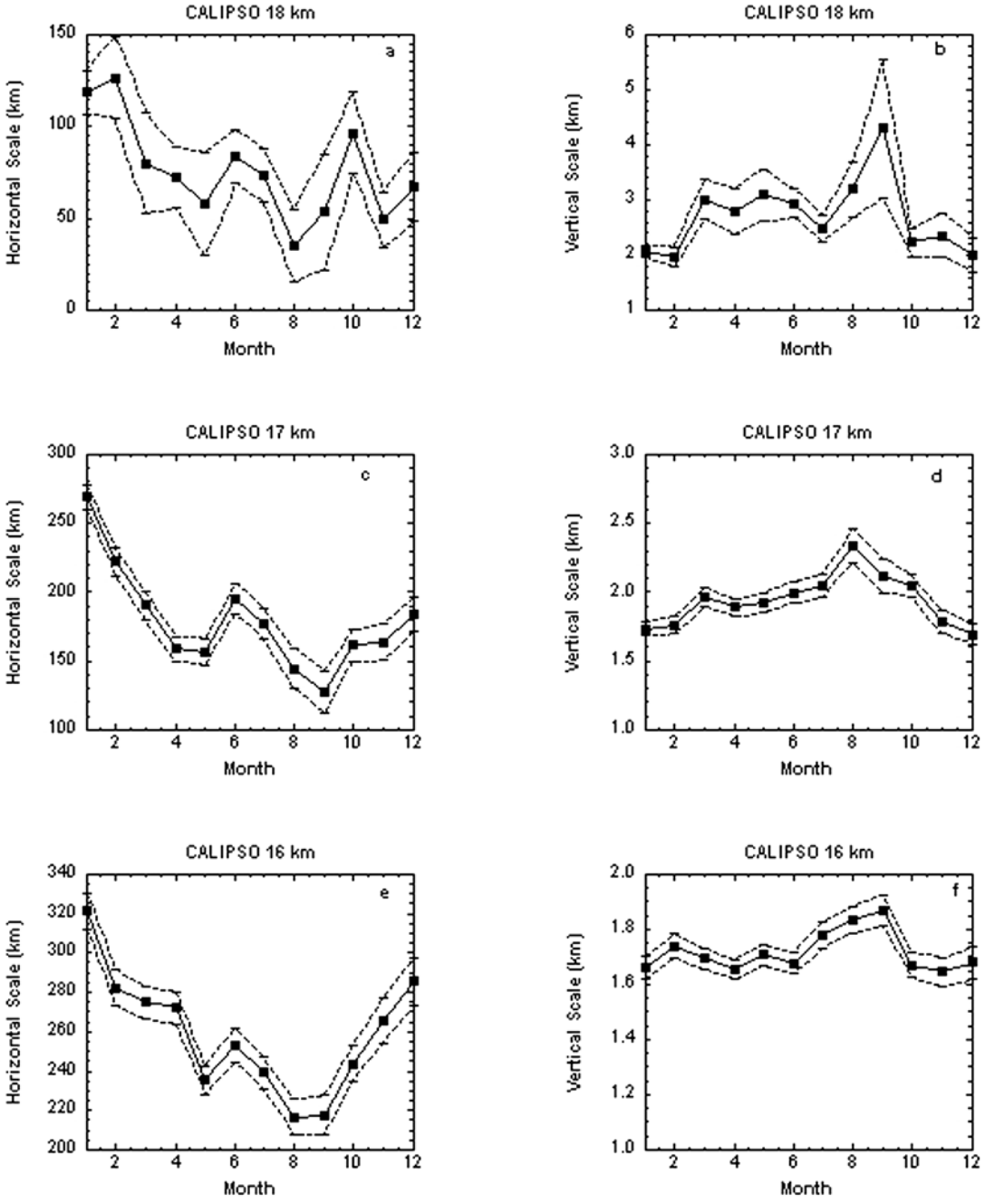


**Figure 13.** CALIPSO monthly averages of (left) horizontal and (right) vertical scales in the tropics. Dotted curves specify the 95% confidence intervals of the means.

for the range between 0.1 and 0.2 km. Approximately half of the vertical depths occur for depths less than 1.2 km at 16 and 17 km. The numbers of observations at 18 km altitude for vertical depth bins near 1 km (~150) are substantially less than for the bins at 16 and 17 km (~2000 and 1000, respectively). This accounts for the jagged appearance of the 18 km probability distribution function (pdf). The pdfs peak for vertical depths between 0.8 and 1.0 km.

[41] Figure 13 presents monthly averages of CALIPSO horizontal and vertical depths for 30°S to 30°N at 16, 17, and 18 km altitude. Means are indicated in Figure 13 by the solid squares. As mentioned in the previous paragraph, there are 10 times fewer data points at 18 km than at the other altitudes, and the dotted curves in Figure 13 (which specify the 95% confidence intervals of the means) reflect this fact. In general, horizontal scales are largest in winter, and smallest in August–September. Vertical depth means vary by a few tenths of a kilometer at each altitude.

[42] A possible reason why horizontal scales are longest in winter is that the horizontal distances between deep convective centers are largest in winter (December–February). The positions of deep convection in winter and summer, as indicated by CDC OLR values less than 170 W $m^{-2}$, are separated by approximately 2070 and 1600 km,

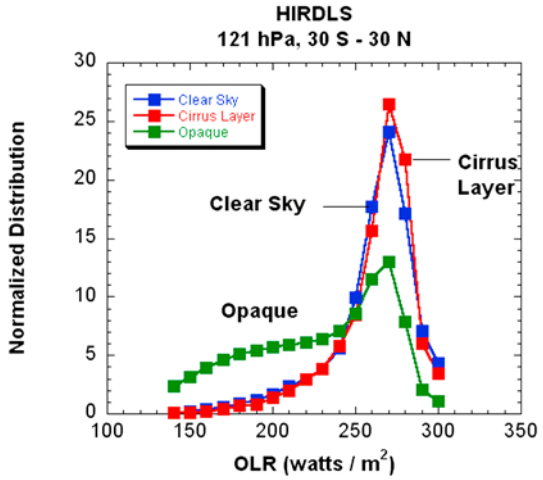


**Figure 14.** Normalized distributions of clear sky, opaque, and isolated cirrus layers observed by HIRDLS at 121 hPa for 30°S–30°N as a function of Climate Diagnostic Center OLR. Opaque clouds are associated with lower OLR (i.e., convective clouds). The time period is from 21 January 2005 through 31 December 2007.

respectively, for the longitude and latitude range in which isolated cirrus is observed (i.e., 50 to 210° longitude, 25°S to 10°S, and 15°N to 25°N; see Figure 5). Deep convection will disrupt isolated cirrus that has a long horizontal scale.

## 6. Relation to OLR

[43] The locations of deep convection in the tropics changes on a day to day basis. It is therefore useful to calculate normalized distributions of OLR versus cirrus type and depths that can be used to validate climate models that calculate cirrus structure. Cirrus is formed directly by deep convection, the dissipation stage of deep convection, the uplifting of humid layers (i.e., formed in situ), and by localized cold pockets associated with dynamical waves. Models that account for all of these sources likely will have a better chance of agreeing with observed statistical distributions than models that do not account for the source mechanisms.

[44] Figures 14 and 15 present normalized distributions of HIRDLS and CALIPSO cirrus statistics at 121 hPa and 15 km altitude, respectively, presented as a function of Climate Diagnostic Center OLR. Figure 14 was calculated using the HIRDLS cloud flags (0 for clear skies, 2 for cirrus layers, and 4 for opaque clouds) for the time period 21 January 2005 through 31 December 2007. The normalized pdfs show that the isolated cirrus layers are predominantly associated with OLR regions similar to clear sky regions. This is reasonable, since thin cirrus at altitudes near the tropopause, accompanied with clear sky regions below the isolated layer, has a very small vertical optical depth, and little effect upon OLR.

[45] Figure 15 displays CALIPSO vertical depths as a function of OLR at 15 km altitude for the time period 1 September 2006 through 31 August 2007. Thinner cirrus is associated with larger pdf values for clear skies (i.e., OLR near 270 W/m$^2$). Thicker cirrus is associated with lower OLR values associated with extensive cloud structure (i.e., OLR less than 200 W/m$^2$). In Figure 16 the pdfs are presented as a function of horizontal length for observations at 16 km altitude. The longest cirrus structures (laminar cirrus) are associated with clear skies, while shorter scales dominant over convective regions (low OLR).

## 7. Conclusions

[46] The similarities in the seasonal HIRDLS and CALIPSO cloud frequency of occurrence in the upper

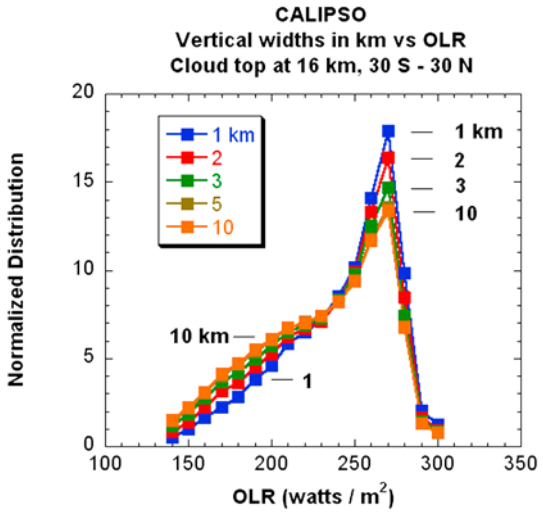


**Figure 15.** The pdfs of CALIPSO cloud observation frequency as a function of Climate Diagnostic Center OLR and vertical depth for the time period 1 September 2006 through 31 August 2007. Clouds with larger vertical depth are associated with lower OLR (convective clouds) while thinner depths are observed over clear skies. The pdfs are calculated for vertical depths with the ranges of [0.2, 1], [0.2, 2], [0.2, 3], [0.2, 5], and [0.2, 10].

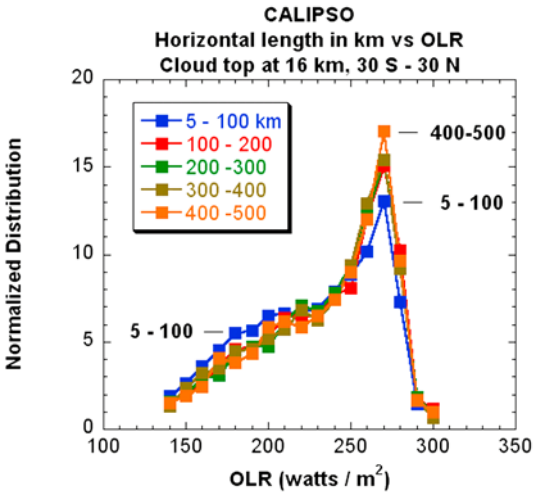


**Figure 16.** The pdfs of CALIPSO cloud observation frequency as a function of Climate Diagnostic Center OLR and horizontal length for the time period 1 September 2006 through 31 August 2007. Clouds with smaller horizontal lengths are associated preferentially with lower OLR (convective clouds), while longer horizontal lengths are associated with clear skies.

troposphere in the tropics (Figures 1–3) indicates that these two experiments are observing similar time-averaged cloud structure. In agreement with previous studies [*Wang et al.*, 1996; *Mergenthaler et al.*, 1999; *Fu et al.*, 2007], the cirrus frequency of occurrence falls off sharply as the tropopause is encountered. Isolated laminar cirrus is located away from the maritime continent, (i.e., away from deep convection, see Figures 3 and 5).

[47] Studies using previous solar occultation, limb-emission and lidar data [*Wang et al.*, 1996; *Winker and Trepte*, 1998; *Mergenthaler et al.*, 1999; *Massie et al.*, 2003] did not have the temporal sampling necessary to observe cirrus on a monthly basis. Solar occultation experiments measure 32 profiles per day, while the HIRDLS experiment measures ~5500 profiles per day, and the CALIPSO CALIOP lidar produces a footprint every 333m along the orbital track (~120,000 profiles per day). The improved sampling makes possible the detailed study of individual monthly averaged features (see Figures 6 and 7). The details correlate well with MLS RHI data (see Figure 8), though the 5 km field of view of MLS does produce RHI less than 100% for observation geometries in which kilometer-thick cirrus is present. As presented in Figure 12, approximately 50% of the cirrus in the upper troposphere has a vertical depth less than 1.2 km. Pdfs of vertical depth peak between 0.8 and 1.0 km.

[48] While the LITE experiment [*Winker and Trepte*, 1998] during 10–19 September 1994 was able to determine the frequency of occurrence (~7%) of laminar cirrus, the determination of monthly variations of horizontal structures awaited the launch of the CALIPSO-CALIOP lidar. Horizontal lengths in the upper troposphere are longest in winter, and shortest in August–September (see Figure 13).

[49] The CALIPSO and HIRDLS data presented in this paper are archived in IDL savesets and netCDF files at discrete altitude and pressure levels, respectively. These cloud frequency data, expressed on a seasonal and monthly basis in the tropics, and the statistics of the horizontal and vertical depths (Figures 13–16) will be useful for validation studies of climate models. Observed cirrus is produced by different sources: deep convection, dissipative convection, and in situ formation processes. There will likely be differences in observed and model statistical distributions of the cirrus, expressed as a function of OLR, if all of the formation processes are not properly accounted for in climate models.

[50] **Acknowledgments.** This research is supported by NASA grant NNX08AN76G and the NASA HIRDLS project at NCAR. NCAR is sponsored by the National Science Foundation. MLS data were produced at the Jet Propulsion Laboratory at California Institute of Technology under contract with the National Aeronautics and Space Administration. Appreciation is expressed to Eric Jensen, Charles Bardeen, and Debbie Mao for helpful reviews of the paper. This paper is dedicated to the memory of John L. Mergenthaler.

## References

Comstock, J. M., T. P. Ackerman, and G. G. Mace (2002), Ground-based lidar and radar remote sensing of tropical cirrus clouds at Nauru Island: Cloud statistics and radiative impacts, *J. Geophys. Res.*, *107*(D23), 4714, doi:10.1029/2002JD002203.

Corti, T., B. P. Luo, T. Peter, H. Vomel, and Q. Fu (2005), Mean radiative energy balance and vertical mass fluxes in the equatorial upper troposphere and lower stratosphere, *Geophys. Res. Lett.*, *32*, L06802, doi:10.1029/2004GL021889.

Corti, T., B. P. Luo, Q. Fu, H. Vomel, and T. Peter (2006), The impact of cirrus clouds on tropical troposphere-to-stratosphere transport, *Atmos. Chem. Phys.*, *6*, 2539–2547.

Dessler, A. E., S. P. Palm, W. D. Hart, and J. D. Spinhirne (2006a), Tropopause-level thin cirrus coverage revealed by ICESat/Geoscience Laser Altimeter System, *J. Geophys. Res.*, *111*, D08203, doi:10.1029/2005JD006586.

Dessler, A. E., S. P. Palm, and J. D. Spinhirne (2006b), Tropical cloud-top height distributions revealed by the Ice, Cloud, and Land Elevation Satellite (ICESat)/Geoscience Laser Altimeter System (GLAS), *J. Geophys. Res.*, *111*, D12215, doi:10.1029/2005JD006705.

Fu, Q., Y. Hu, and Q. Yang (2007), Identifying the top of the tropical tropopause layer from vertical mass flux analysis and CALIPSO lidar cloud observations, *Geophys. Res. Lett.*, *34*, L14813, doi:10.1029/2007GL030099.

Gille, J., et al. (2008), High Resolution Dynamics Limb Sounder: Experiment overview, recovery, and validation of initial temperature data, *J. Geophys. Res.*, *113*, D16S43, doi:10.1029/2007JD008824.

Jensen, E., and L. Pfister (2004), Transport and freeze-drying in the tropical tropopause layer, *J. Geophys. Res.*, *109*, D02207, doi:10.1029/2003JD004022.

Khosravi, R., et al. (2009), Overview and characterization of retrievals of temperature, pressure, and atmospheric constituents from the High Resolution Dynamics Limb Sounder (HIRDLS) measurements, *J. Geophys. Res.*, *114*, D20304, doi:10.1029/2009JD011937.

Kim, S.-W., S. Berthier, J.-C. Raut, P. Chazette, F. Dulac, and S.-C. Yoon (2008), Validation of aerosol and cloud layer structures from the space-borne lidar CALIOP using a ground-based lidar in Seoul, Korea, *Atmos. Chem. Phys.*, *8*, 3705–3720.

Kinnison, D. E., et al. (2008), Global observations of $HNO_3$ from the High Resolution Dynamics Limb Sounder (HIRDLS): First results, *J. Geophys. Res.*, *113*, D16S44, doi:10.1029/2007JD008814.

Lawson, R. P., B. Pilson, B. Baker, Q. Mo, E. Jensen, L. Pfister, and P. Bui (2008), Aircraft measurements of microphysical properties of subvisible cirrus in the tropical tropopause layer, *Atmos. Chem. Phys.*, *8*, 1609–1620.

Liebmann, B., and C. A. Smith (1996), Description of a complete (interpolated) outgoing longwave radiation dataset, *Bull. Am. Meteorol. Soc.*, *77*, 1275–1277.

List, R. J. (1951), *Smithsonian Meteorological Tables*, *Smithsonian Misc. Collect.*, vol. 114, Smithsonian Inst., Washington, D. C.

Liu, Z., M. Vaughan, D. Winker, C. A. Hostetler, L. R. Poole, D. L. Hlavka, W. D. Hart, and M. J. McGill (2004), Use of probability distribution functions for discriminating between cloud and aerosol in lidar backscatter data, *J. Geophys. Res.*, *109*, D15202, doi:10.1029/2004JD004732.

Lynch, D. K., and K. Sassen (2002), Subvisual cirrus, in *Cirrus*, edited by D. K. Lynch et al., pp. 256–264, Oxford Univ. Press, New York.

Massie, S., W. Randel, F. Wu, D. Baumgardner, and M. Hervig (2003), Halogen Occultation Experiment and Stratospheric Aerosol and Gas Experiment II observations of tropopause cirrus and aerosol during the 1990s, *J. Geophys. Res.*, *108*(D7), 4222, doi:10.1029/2002JD002662.

Massie, S., et al. (2007), High Resolution Dynamics Limb Sounder observations of polar stratospheric clouds and subvisible cirrus, *J. Geophys. Res.*, *112*, D24S31, doi:10.1029/2007JD008788.

Mergenthaler, J. L., A. E. Roche, J. B. Kumer, and G. A. Ely (1999), Cryogenic Limb Array EtaIon Spectrometer observations of tropical cirrus, *J. Geophys. Res.*, *104*(D18), 22,183–22,194, doi:10.1029/1999JD900397.

Nardi, B., et al. (2008), Initial validation of ozone measurements from the High Resolution Dynamics Limb Sounder, *J. Geophys. Res.*, *113*, D16S36, doi:10.1029/2007JD008837.

Omar, A. H., and C. S. Gardner (2001), Observations by the Lidar In-Space Technology Experiment (LITE) of high-altitude cirrus over the equator in regions exhibiting extremely cold temperatures, *J. Geophys. Res.*, *106*(D1), 1227–1236, doi:10.1029/2000JD900489.

Randel, W. J., R. Garcia, and F. Wu (2008), Dynamical balances and tropical stratospheric upwelling, *J. Atmos. Sci.*, *65*, 3584–3595, doi:10.1175/2008JAS2756.1.

Read, W. G., et al. (2007), Aura Microwave Limb Sounder upper tropospheric and lower stratospheric $H_2O$ and relative humidity with respect to ice validation, *J. Geophys. Res.*, *112*, D24S35, doi:10.1029/2007JD008752.

Sassen, K. (2002), Cirrus: A modern perspective, in *Cirrus*, edited by D. K. Lynch et al., pp. 11–40, Oxford Univ. Press, New York.

Vaughan, M., S. Young, D. Winker, K. Powell, A. Omar, A. Liu, Y. Hu, and C. Hostetler (2004), Fully automated analysis of space-based lidar data: An overview of the CALIPSO retrieval algorithms and data products, *Proc. SPIE Int. Soc. Opt. Eng.*, *5575*, 16–30.

Vaughan, M., D. Winker, and K. Powell (2005), CALIOP algorithm theoretical basis document—Part 2: Feature detection and layer properties

algorithms, *PC-SCI-202 Part 2*, NASA Langley Res. Cent., Hampton, Va. (Available at http://www-calipso.larc.nasa.gov/resources/project_documentation.php)

Wang, L., and A. E. Dessler (2006), Instantaneous cloud overlap statistics in the tropical area revealed by ICESat/GLAS data, *Geophys. Res. Lett.*, *33*, L15804, doi:10.1029/2005GL024350.

Wang, P.-H., P. Minnis, P. M. Cormick, G. Kent, and K. Skeens (1996), A 6-year climatology of cloud occurrence frequency from Stratospheric Aerosol and Gas Experiment II observations (1985–1990), *J. Geophys. Res.*, *101*(D23), 29,407–29,429, doi:10.1029/96JD01780.

Winker, D. M., and C. R. Trepte (1998), Laminar cirrus observed near the tropical tropopause by LITE, *Geophys. Res. Lett.*, *25*(17), 3351–3354, doi:10.1029/98GL01292.

Winker, D. M., W. H. Hunt, and M. J. McGill (2007), Initial performance assessment of CALIOP, *Geophys. Res. Lett.*, *34*, L19803, doi:10.1029/2007GL030135.

J. Barnett, Department of Atmospheric, Oceanic and Planetary Physics, Oxford University, Parks Road, Oxford OX1 3PU, UK. (j.barnett1@physics.ox.ac.uk)

C. Craig, J. Gille, R. Khosravi, and S. T. Massie, Atmospheric Chemistry Division, National Center for Atmospheric Research, PO Box 3000, Boulder, CO 80307, USA. (cacraig@ucar.edu; gille@ucar.edu; Rashid@ucar.edu; massie@ucar.edu)

W. Read, Jet Propulsion Laboratory, California Institute of Technology, MS 183-701, 4800 Oak Grove Dr., Pasadena, CA 91109, USA. (bill@mls.jpl.nasa.gov)

D. Winker, NASA Langley Research Center, MS 475, Hampton, VA 23681, USA. (dmwinker@gmail.com)